PCCP

PAPER

Cite this: *Phys. Chem. Chem. Phys.*, 2015, **17**, 7498

The effect of an oligonucleotide on the structure of cationic DODAB vesicles

Julio H. K. Rozenfeld,* Evandro L. Duarte, Leandro R. S. Barbosa and M. Teresa Lamy

Received 4th December 2014,
Accepted 12th February 2015

DOI: 10.1039/c4cp05652c

www.rsc.org/pccp

The effect of a small single-stranded oligonucleotide (ODN) on the structure of cationic DODAB vesicles was investigated by means of differential scanning calorimetry (DSC), small angle X-ray scattering (SAXS) and electron spin resonance (ESR) spectroscopy. ODN adsorption induced coalescence of vesicles and formation of multilamellar structures with close contact between lamellae. It also increased the phase transition temperature by 10 °C but decreased transition cooperativity. The ODN rigidified and stabilized the gel phase. In the fluid phase, a simultaneous decrease of ordering close to the bilayer surface and increase in bilayer core rigidity was observed in the presence of the ODN. These effects may be due not only to electrostatic shielding of DODAB head groups but also to superficial dehydration of the bilayers. The data suggest that oligonucleotides may induce the formation of a multilamellar poorly hydrated coagel-like phase below phase transition. These effects should be taken into account when planning ODN delivery employing cationic bilayer carriers.

1. Introduction

Small single-stranded oligonucleotides (ODNs) can promote the repair of DNA point mutations[1] and silence specific genes.[2] Antisense ODNs that inhibit the expression of proteins inside a cell have been used both as tools for basic research on gene expression and function[3,4] and as therapeutic agents.[5,6] Indeed, ODNs have been employed in vaccine design[7] and in the treatment of allergy[8] and cancer.[9]

In order to avoid obstacles such as degradation and poor capture by target cells, ODNs need suitable carriers for effective delivery.[10,11] Liposomes, for instance, have been successfully employed as ODN carriers,[12] especially after the development of cationic lipids.[13,14]

Dioctadecyldimethylammonium bromide (DODAB) is a synthetic cationic lipid formed by two 18-carbon alkyl chains attached to a quaternary ammonium group. Its cylindrical geometry allows the formation of different structures in aqueous solutions: large vesicles are produced by chloroform vaporization[15] and heating above phase transition temperature;[16] small open bilayer fragments are produced by sonication.[17,18]

DODAB bilayers are very versatile: they have been used as templates for polymerization and deposition of materials,[19] as hydrophobic drug carriers[20,21] and as microbicides.[22] DODAB was also employed in the production of biomimetic particles[23] and in the design of vaccines.[24]

DODAB has also been successfully employed as a DNA carrier,[25] which opened the possibility of applying it as an oligonucleotide carrier. In this context, it was recently demonstrated that stable assemblies of DODAB bilayers and immunostimulatory CpG ODNs induce the formation of very strong and specific immune responses,[26] allowing the development of novel vaccine adjuvants.

The aim of this work was to investigate the effect of an oligonucleotide on the structure of DODAB vesicles. The resulting ODN–DODAB assemblies were characterized by means of differential scanning calorimetry (DSC), small angle X-ray scattering (SAXS) and electron spin resonance (ESR) spectroscopy.

2. Materials and methods

2.1. Materials

Dioctadecyldimethylammonium bromide (DODAB) 99.9% pure was purchased from Sigma Chemical Co. (St Louis, MO, USA). The ten-base single-stranded oligonucleotide 3′-AAA AAAAAA A-5′ (ODN) was purchased from Integrated DNA Technologies IDT (Coralville, IA, USA). Spin labels 1-palmitoyl-2-(*n*-doxylsearoyl)-*sn*-*glycero*-3-phosphocholine (*n*-PCSL, *n* = 5 or 16) were supplied by Avanti Polar Lipids (Birmingham, AL, USA). Ultrapure water of Milli-Q-Plus quality was used throughout. The chemical structures of DODAB, 5- and 16-PCSL are shown in Fig. 1.

2.2. Preparation of ODN stock solutions, DODAB vesicles and ODN–DODAB assemblies

Lyophilized ODN was solubilized in ultrapure water to produce 10 mM stock solutions.

Instituto de Física, Universidade de São Paulo, São Paulo, Brazil.
E-mail: julioroz@if.usp.br; Tel: +55 11 3091 6829

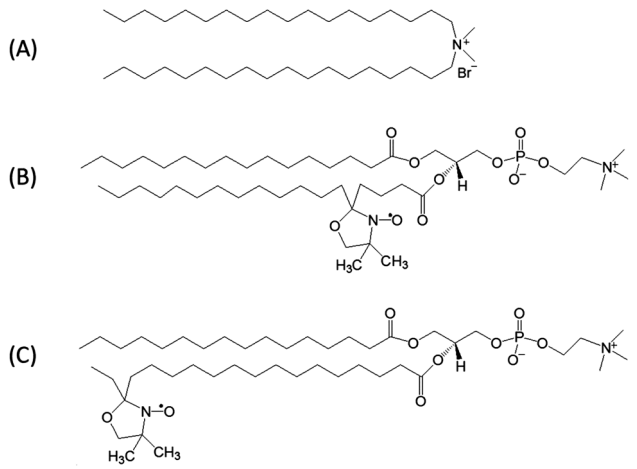

Fig. 1 Chemical structures of DODAB (A), 5-PCSL (B) and 16-PCSL (C).

DODAB lipid films were formed from chloroform solutions, dried under a stream of N_2, and left under reduced pressure for a minimum of 2 h to remove all traces of organic solvent. Vesicles were prepared by adding water to the films and heating them for 30 min at 60 °C, *i.e.*, above the phase transition temperature. Heating was accompanied by vigorous vortexing at about every 10 minutes in order to ensure a homogenous dispersion. Concentration of DODAB stock dispersions were typically 3 mM, as analytically determined by halide microtitration.[27] For ESR experiments, 0.8 mol% 5-PCSL or 0.3 mol% 16-PCSL were added to the chloroform solutions when preparing the lipid films. No spin–spin interaction was observed for such small label concentrations.

ODN–DODAB assemblies were prepared after cooling the vesicles at room temperature. Suitable volumes of water, vesicles and ODN were mixed and the lipoplexes formed were incubated for 24 h prior to measurements. The final concentrations were 2 mM DODAB and 0.4 mM ODN.

2.3. Differential scanning calorimetry (DSC)

DSC scans were performed in a Microcal VP-DSC Microcalorimeter (Microcal Inc., Northampton, MA, USA) equipped with 0.5 mL twin total-fill cells. The heating rates were 20 °C h^{-1} (10 °C h^{-1} yielded identical scans). Scans were performed at least in duplicate. Thermograms correspond to the second upscan. Transition enthalpies (ΔH) were obtained by integrating the area under the thermograms along the 20 °C to 60 °C range.

2.4. Small angle X-ray scattering (SAXS)

Measurements were performed in the SAXS1 beam line of the LNLS (National Synchrotron Radiation Laboratory, Campinas, SP, Brazil). The X-ray wavelength used was λ = 1.55 Å, and the SAXS sample-to-detector distance was around 600 mm. A bidimensional PILATUS 300k detector was used. Samples were set between two flat Mica walls with a 1 mm spacer. A thermal bath was used for temperature control. Data were normalized for the acquisition time (120 s) and checked for radiation damage. The final scattering curves were subtracted from the aqueous solution and corrected by the sample's attenuation. Repeat distances (d) were calculated using the well-known repetition distance for lamellar structures, $d = \frac{2\pi}{q_{peak}}$, where $q = \frac{4\pi}{\lambda}\sin\theta$ is the scattering vector and 2θ the scattering angle.

The SAXS data analysis for multilamellar structures should take into account the contribution of both DODAB and ODN. In this case, the scattering intensity of a set of stacked bilayers with ODN molecules present between two adjacent bilayers can be written as a weighted sum of each individual contribution, as follows:

$$I(q) = k\left(w_1\frac{P_t(q)S(q)}{q^2} + w_2 P_{ODN}(q)\right)$$

where k is related to the experimental setup; $P_t(q)$ is the bilayer cross-section form factor (perpendicular to the membrane plane); $P_{ODN}(q)$ is the form factor of ODN; $S(q)$ is the structure factor; and w_1 and w_2 are the weights of the stacked bilayers and the ODN, respectively.

$P_t(q)$ can be modeled by assuming that the membrane is composed of three different layers: a polar headgroup (encompassing the ODN when present), paraffinic chains and the methyl group. Each layer has a distinct electron density with respect to the solvent (ρ_{sol} = 0.33 e $Å^{-3}$ for water solution): ρ_{pol} is the electron density for the polar headgroup, ρ_{CH_2} for the paraffinic tails and ρ_{CH_3} for the methyl group. Similarly, each layer has its own thickness: R_{pol} for the polar headgroup, R_{CH_2} for the paraffinic chains and R_{CH_3} for the methyl group.

During the fitting procedure, some of these parameters were allowed to vary within a narrow range: R_{CH_3} (0.15 nm < R_{CH_3} < 0.35 nm), ρ_{CH_3} (150 e nm^{-3} < ρ_{CH_3} < 200 e nm^{-3}) and ρ_{par} (250 e nm^{-3} < ρ_{par} < 330 e nm^{-3}), in accordance with data from the literature.[28,29] The other $P_t(q)$ parameters were allowed to vary in a corresponding broader range. A more detailed description of this model can be found elsewhere.[28]

The structure factor $S(q)$ is equal to 1 for non-interacting systems. However, for multilamellar structures, the Modified Caillé Theory (MCT) can be applied.[30–32] It takes into account the bending of the bilayers in addition to the fluctuations in the space between bilayers, through a disorder parameter, $\eta_{Caillé}$.[31] In this model, $S(q)$ can be written as[31]

$$S(q) = N + 2\left\{\sum_{n=1}^{N-1}(N-n)\cos(nqd)e^{-0.5772\eta\left(\frac{qd}{2\pi}\right)^2}(\pi n)^{-\eta\left(\frac{qd}{2\pi}\right)^2}\right\}$$

where N is the number of stacked bilayers, d is the repetition distance and η is the Caillè parameter, which involves the bending modulus K of lipid bilayers and the bulk modulus B for compression, and can be written as[31,33]

$$\eta = \frac{\pi k_B T}{2d^2\sqrt{KB}}$$

During the fitting process two parameters were varied: N and η, whereas d was calculated as explained earlier in the text.

ODN molecules were considered as rigid cylinders with cross-section and length equal to 0.6(2) nm and 3.4(3) nm,

respectively, according to data available in the literature for an oligonucleotide with the same number of 10 nucleotides.[34]

All scattering curves were analyzed with the global fitting methodology using GENFIT software.[35]

2.5. ESR spectroscopy

ESR measurements at X-band were performed using a Bruker EMX spectrometer. Field-modulation amplitude of 1G and microwave power of 5 mW were used. The temperature was controlled to about 0.2 °C with a Bruker BVT-2000 variable temperature device, and monitored using a Fluke 51 K J^{-1} thermometer with a probe placed just above the cavity. A high sensitivity ER4119HS cavity was used. All ESR data shown are means of the results of at least two experiments, and the uncertainties are the standard deviations. When not shown, the uncertainty was found to be smaller than the symbol in the graph.

The effective order parameter, S_{eff}, was calculated from the expression[36]

$$S_{\mathrm{eff}} = \frac{A_{\parallel} - A_{\perp}}{A_{zz} - (1/2)(A_{xx} + A_{yy})} \frac{a_{\mathrm{o}}'}{a_{\mathrm{o}}}$$

where $a_{\mathrm{o}}' = (1/3)(A_{xx} + A_{yy} + A_{zz})$, $a_{\mathrm{o}} = (1/3)(A_{\parallel} + 2A_{\perp})$, $A_{\parallel}$ ($= A_{\mathrm{max}}$) is the maximum hyperfine splitting directly measured on the spectrum (see Fig. 5), $A_{\perp} = A_{\mathrm{min}} + 1.4\left[1 - \frac{A_{\parallel} - A_{\mathrm{min}}}{A_{zz} - (1/2)(A_{xx} + A_{yy})}\right]$, A_{min} is the measured inner hyperfine splitting (see Fig. 4) and A_{xx}, A_{yy} and A_{zz} are the principal values of the hyperfine tensor for doxylpropane.[37]

The ratio between the high and central field line amplitudes (h_{-1}/h_0) was also directly taken from the spectra (see Fig. 6).

2.6. Vesicle coalescence assay

Two stock solutions of DODAB were prepared as previously described (see Section 2.2.): one was labeled with 2 mol% 16-PCSL and the other was unlabeled. Aliquots of the stock solutions were mixed in order to obtain a mixture of 0.2 mM labeled vesicles plus 1.8 mM unlabeled vesicles, *i.e.*, a final lipid concentration of 2 mM and a final 0.2 mM labeled/1.8 mM unlabeled vesicle ratio. The volume was completed to 80 μL using water or an aliquot from a 10 mM ODN stock solution. In this case, the final ODN concentration was 0.4 mM. Samples were incubated for 1 hour at room temperature and then heated and incubated for 10 minutes at 60 °C. After incubation, the ESR spectra were recorded at 60 °C. At this temperature, the ESR signal is rather narrow, clearly allowing the detection of any broadening due to spin–spin exchange.

3. Results

3.1. ODN increases the gel-fluid transition temperature by 10 °C but decreases the transition cooperativity and enthalpy

The thermotropic behavior of DODAB bilayers in the presence or absence of ODN is shown in Fig. 2.

In the absence of ODN, DODAB displays a narrow phase transition at 44 °C. This narrow peak at 44 °C is characteristic of a very cooperative process, in which lipid molecules do not melt independently of each other due to strong lipid–lipid interactions. The transition cooperativity is related to the temperature range in which the transition takes place; the narrower the temperature range, the more cooperative the transition is.[38] In the presence of ODN, the endothermic peak at 44 °C disappears and a broader and less intense peak appears at 54 °C (Fig. 2). The broadening of the peak indicates a less cooperative phase transition.

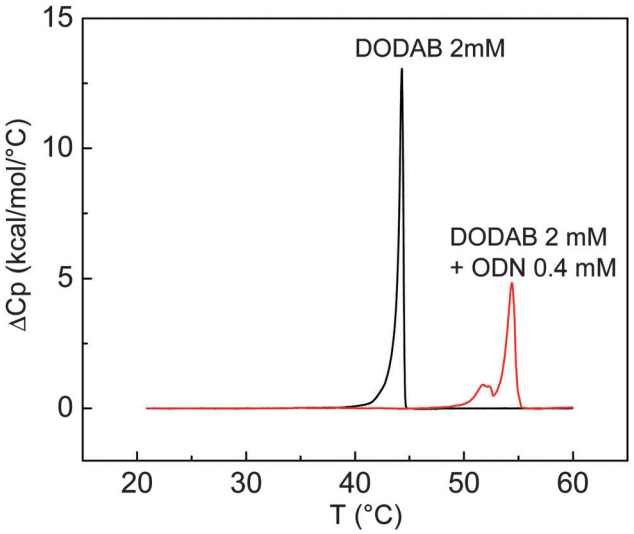

Fig. 2 Effect of 0.4 mM ODN on DSC scan for 2 mM DODAB vesicles. Heating rate was 20 °C h^{-1}.

Table 1 Transition enthalpies (ΔH) of 2 mM DODAB vesicles in absence or presence of 0.4 mM ODN (standard deviation in parenthesis)

Dispersion	ΔH (kcal mol^{-1})
DODAB	9.4 (1)
DODAB + ODN	6.8 (1)

Table 1 shows the transition enthalpies (ΔH) calculated from thermograms in Fig. 2. ΔH values decrease 28% in the presence of oligonucleotides.

3.2. ODN induces coalescence of DODAB vesicles into multilamellar structures

Vesicles marked with excess spin labels present a broad ESR spectrum that is characteristic of spin exchange interactions.[39] Fig. 3 shows that this broad spectrum does not change by mixing labeled and unlabeled vesicles, showing that there is no spontaneous vesicle coalescence.

However, the addition of ODN to the mixture of labeled and unlabeled vesicles led to a narrowing of the spectrum that is due to probe dilution within the bilayer phase caused by vesicle coalescence.

This coalescence led to the formation of multilamellar structures, as observed from SAXS spectra (Fig. 4). In the absence of ODN, the scattering profile is characteristic of unilamellar vesicles.[40] On the other hand, in the presence of ODN the scattering

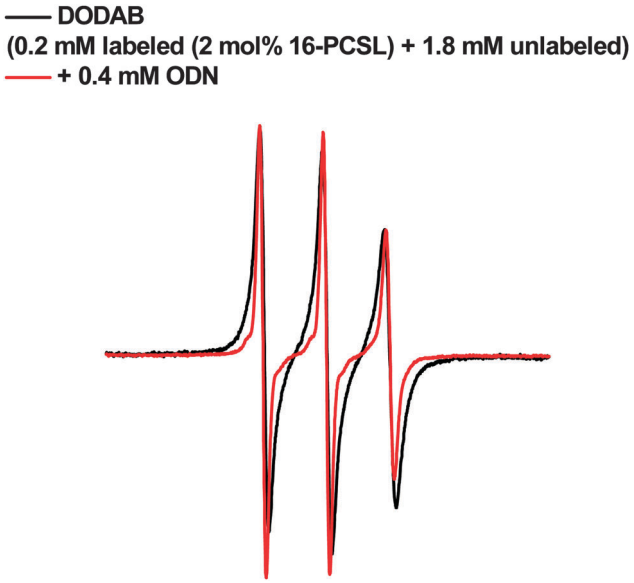

Fig. 3 Effect of ODN on ESR spectrum of mixtures containing spin-labeled and unlabeled DODAB vesicles. Vesicles were labeled with 2 mol% 16-PCSL. A final 0.2 mM labeled/1.8 mM unlabeled vesicle ratio interacted in presence or absence of ODN for 1 hour at room temperature before the ESR spectra were recorded at 60 °C.

curves show Bragg peaks at $\sim$1.41 nm^{-1} and $\sim$2.84 nm^{-1}. This ratio of 1 : 2 for diffraction orders is characteristic of a multilamellar phase.[40]

Along the lipid gel phase, in the temperature range of 20 °C to 35 °C, the first diffraction order in the presence of ODN is conserved at $\sim$1.41 nm^{-1} (Fig. 4), from which it is possible to calculate a repeat distance of $\sim$4.5 nm (see Section 2.4.). On the other hand, in the fluid phase, at 60 °C, the first diffraction order is shifted to $\sim$1.32 nm^{-1} (Fig. 4), resulting in a repeat distance of $\sim$4.8 nm.

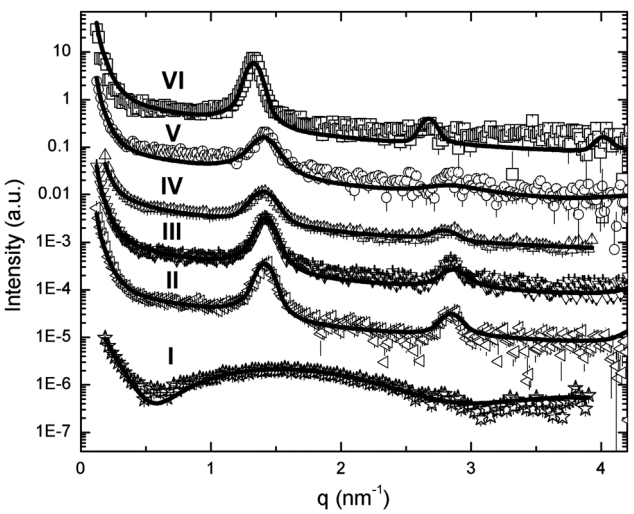

Fig. 4 SAXS curves of 2 mM DODAB in the absence (I) and presence of 0.4 mM ODN (II–VI) at different temperatures: 20 °C (II), 25 °C (III), 30 °C (I and IV), 35 °C (V) and 60 °C (VI).

Table 2 Values of SAXS data analysis using the MCT theory at different temperatures[a]

T (°C)	ODN (mM)	R_{pol} (nm)	R_{CH_2} (nm)	R_{CH_3} (nm)	ρ_{pol} (e nm^{-3})	N	η	r_W (nm)
30	0	0.47(2)	1.1(3)	0.20(1)	470(10)	—	—	—
20	0.4	0.44(2)	1.2(2)	0.30(2)	450(10)	8(1)	0.012	0.5(1)
25	0.4	0.44(2)	1.2(2)	0.30(2)	450(10)	7(1)	0.054	0.5(1)
30	0.4	0.44(3)	1.2(2)	0.30(2)	450(10)	7(1)	0.065	0.5(1)
35	0.4	0.44(3)	1.2(2)	0.30(2)	450(10)	7(1)	0.083	0.5(1)
60	0.4	0.35(2)	1.1(2)	0.20(2)	430(10)	13(1)	0.081	1.4(1)

[a] R_i and ρ_i are the thickness and electron density of the polar headgroup, the CH_2 and CH_3 regions. N is the number of stacked bilayers, η is the Caillè parameter, and r_W is the length of the water thickness between two adjacent bilayers. Standard deviations are in parenthesis.

According to the MCT theory, the number of stacked bilayers was found to be approximately 7 at room temperature, increasing to about 11 at 60 °C (Table 2). The Caillè parameter was found to increase during the increase of temperature, which is in agreement with the literature.[41]

3.3. ODN rigidifies the DODAB gel phase but affects the surface and core of fluid DODAB membranes differently

The effects of ODN on the nanoscopic structure of DODAB bilayers were investigated by means of ESR spectroscopy. This technique probes the environment neighboring the paramagnetic probe attached to the phospholipid acyl chain.[42–44] For instance, 5-PCSL (Fig. 1) is labeled on the 5th carbon of the acyl chain and probes the bilayer close to the water interface, whereas 16-PCSL (Fig. 1) is labeled on the 16th carbon and gives information about the bilayer core. Spectra of 5- and 16-PCSL in DODAB vesicles are shown for different temperatures in Fig. 5 and 6.

In the absence of ODN, the spectra of both probes at 30 °C are typical of nitroxides in a tightly packed environment such as

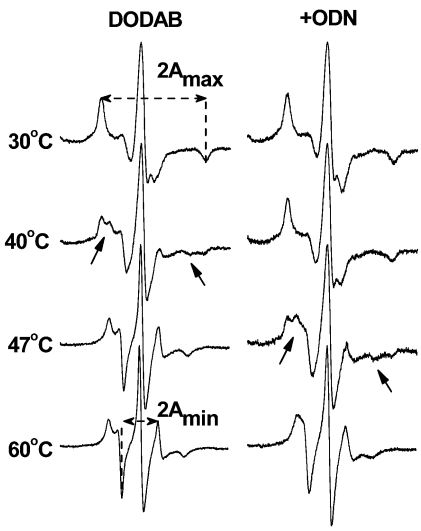

Fig. 5 Effect of 0.4 mM ODN on ESR spectra of 5-PCSL incorporated in 2 mM DODAB vesicles at different temperatures. Dotted lines indicate the position of the maximum and minimum hyperfine splitting (A_{max} and A_{min}). Arrows indicate a more mobile component which coexists with the typical gel phase signal. Total spectra width is 100 G.

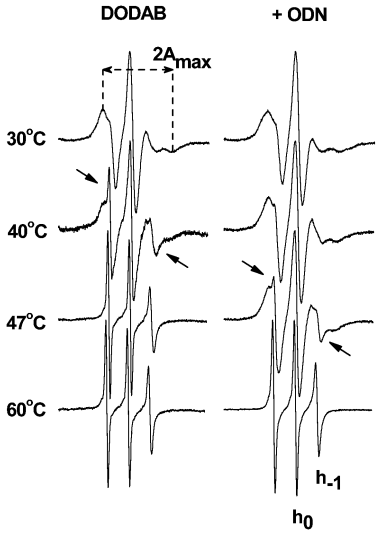

Fig. 6 Effect of 0.4 mM ODN on ESR spectra of 16-PCSL incorporated in 2 mM DODAB vesicles at different temperatures. Maximum hyperfine splitting (A_{max}) is indicated, as well as the position of central (h_0) and high (h_{-1}) field lines. Arrows indicate a more mobile component which coexists with the typical gel phase signal. Total spectra width is 100 G.

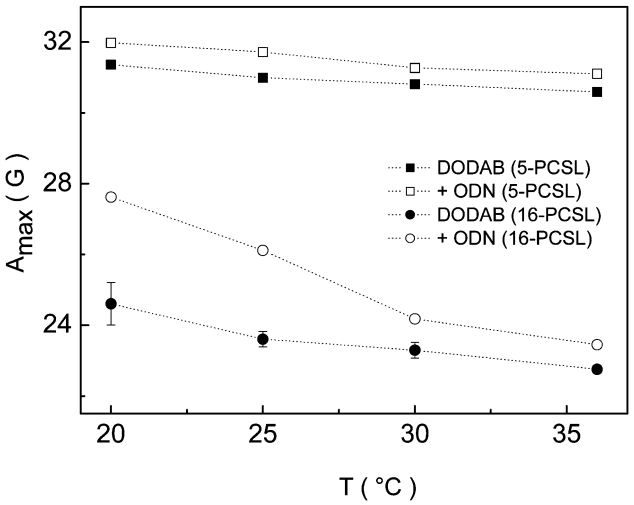

Fig. 7 Effect of ODN on the maximum hyperfine splitting (A_{max}) from ESR spectra of 5- and 16-PCSL incorporated in the gel phase of DODAB vesicles.

the gel phase (Fig. 5 and 6). However, the membranes are less packed in the core than close to the surface. This flexibility gradient towards the bilayer core[37] is evident from the more anisotropic signal of 5-PCSL (Fig. 5) as compared to 16-PCSL (Fig. 6). At 40 °C, there is an evident presence of two signals in the same spectrum for both probes (Fig. 5 and 6). These two signals are characteristic of the coexistence of rigid and fluid lipid domains within the DODAB bilayers.

At 47 °C and 60 °C, the spectra of probes in the absence of ODN are typical of the fluid phase: 5-PCSL is in a rather fluid and ordered location (Fig. 5), close to the bilayer interface, where the labels have fast movement around their long axis;[37] the 16-PCSL spectra indicate fast and nearly isotropic movement for the nitroxide moiety (Fig. 6), typical of the motional narrowing region.[37]

In the presence of ODN, the spectra of 5- and 16-PCSL at 40 °C are very similar to the spectra of pure DODAB at 30 °C (Fig. 5 and 6). The disappearance of the two signals at 40 °C in the presence of ODN indicates that there is only one population of rigid lipids, without the coexistence of rigid and fluid domains.

On the other hand, the spectra in the presence of ODN clearly display two signals at 47 °C (Fig. 5 and 6), indicating the coexistence of fluid and rigid domains at this temperature. At 60 °C, the spectra of both probes are typical of the fluid phase (Fig. 5 and 6).

Empirical parameters obtained from the ESR spectra provide more details on membrane structure. In the gel phase an important parameter is the maximum hyperfine splitting, A_{max} (Fig. 7), which can be directly measured from the ESR spectra and is sensitive to the label environment viscosity or packing.[45]

A_{max} values decrease as the paramagnetic label goes deeper into the bilayer, *i.e.*, A_{max} values for 16-PCSL are smaller than for 5-PCSL (Fig. 7). This reflects the known flexibility gradient towards the bilayer core.[37] In the presence of ODN, A_{max} values are higher for both probes (Fig. 7), indicating that ODN rigidifies the gel phase.

For the fluid phase, distinct parameters should be used to analyze the spectra of each spin label (Fig. 8). The effective order parameter (S_{eff}) is an appropriate parameter to evaluate the acyl chain order with 5-PCSL (Fig. 8A). The position of the nitroxide group closer to the bilayer surface, in an ordered microenvironment, results in anisotropic ESR spectra with clearly defined maximum and minimum hyperfine splittings (A_{max} and A_{min}, respectively). These hyperfine splittings can be directly measured from the ESR spectra (see Fig. 5) and are used to calculate the values of S_{eff},[46] as described in Materials and methods. S_{eff} includes contributions from the chain order and rate of motion, but the main contribution is the amplitude of acyl chains segmental motion.[46]

The slight decrease in S_{eff} values observed in the presence of ODN (Fig. 8A) indicates that ODN adsorption decreases the bilayer order close to the membrane surface in the fluid phase.

Spin labels located deeper into the bilayer, such as 16-PCSL, sense a less ordered microenvironment and yield more isotropic signals from which A_{max} and A_{min} cannot be measured. In this case, the ratio of the amplitudes of the high and central field lines (h_{-1} and h_0 are indicated in Fig. 6) can be evaluated accurately. The h_{-1}/h_0 amplitude ratio tends to unity when the viscosity at the environment probed by the spin label decreases.[43]

The values of h_{-1}/h_0 decrease in the presence of ODN (Fig. 8B), indicating that ODN adsorption rigidifies the core of the DODAB bilayer in the fluid phase. Hence, ODN has different effects on the fluid phase: it decreases the order of the bilayer close to the surface but increases the rigidity of the bilayer core.

4. Discussion

Oligonucleotides spontaneously bind to cationic bilayers due to electrostatic attraction.[10,47] As expected from small single stranded oligonucleotides in water,[34] each ODN molecule used in this work is probably fully charged, with 10 negatively charged phosphates in its backbone, so 0.4 mM ODN would correspond

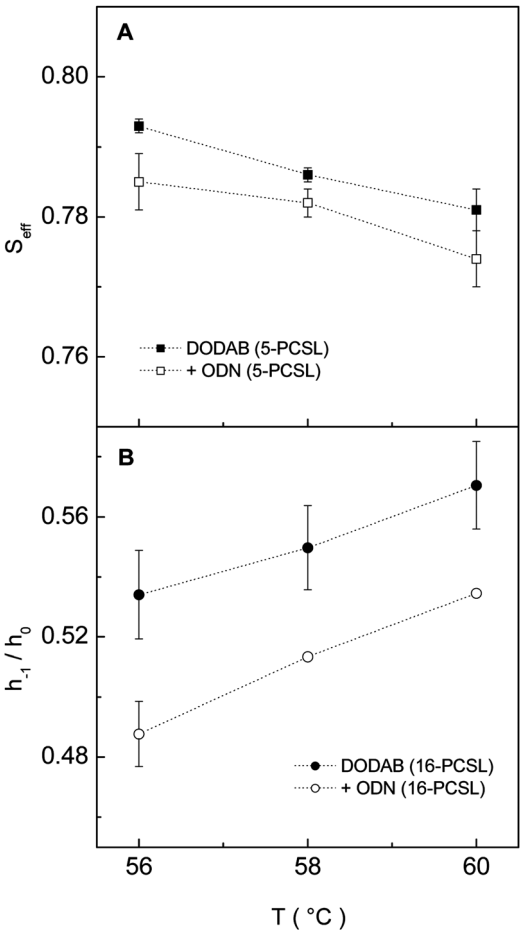

Fig. 8 Effect of ODN on the effective order parameter (S_{eff}) from 5-PCSL ESR spectra (A) and on h_{-1}/h_0 ratios from 16-PCSL ESR spectra (B) of fluid phase DODAB vesicles.

to 4 mM negative charges. This is a condition of excess negative charge, since less than 2 mM DODAB positive charges are available for interaction due to bromide counterion association. The maximum ODN loading obtained at this condition would be useful for biological applications.

The thermotropic behavior of DODAB bilayers has been extensively investigated.[48–51] A cooperative narrow phase transition at 44 °C (Fig. 2) is well established for DODAB vesicles in water.[52,53] Besides the gel and fluid phases, DODAB may present a subgel[52,54] or a coagel[55,56] phase depending on the sample history.

The subgel phase is obtained by cooling the bilayers below 15 °C.[52,54] This phase results from a further stretching and increase in packing of the alkyl chains when compared to the gel phase, and presents a characteristic pre-transition at 36 °C in DSC thermograms.[52,54]

The coagel phase has been observed for samples that were frozen at −20 °C or for concentrated (above 5 mM) DODAB samples.[55,56] This phase corresponds to poorly hydrated multilamellar polycrystalline DODAB suspensions, and results from a loss of the interlamellar water layer, accompanied by a partial dehydration of the lipid headgroups and a further ordering of the hydrocarbon tails.[55,56] It presents a characteristic endothermic peak at 54 °C in heating thermograms.[56]

In the present work, the diluted (2 mM) DODAB samples were not cooled below 20 °C; therefore, no characteristic subgel peak at 36 °C was observed (Fig. 2). However, in the presence of ODN, the endothermic peak shifted from 44 °C to 54 °C. A similar shift was described for small sonicated DODAB bilayer fragments interacting with ODN[43] and for DODAB vesicles interacting with large double stranded DNA molecules.[57] The 10 °C increase in the phase transition temperature suggests that ODN is able to stabilize the DODAB gel phase, and this could be attributed to the shielding of electrostatic repulsion between cationic headgroups by anionic ODN phosphates. However, electrostatic shielding is not the only driving force behind thermotropic behavior changes upon polyelectrolyte adsorption, since ODN was shown to decrease the phase transition temperature of interdigitated cationic diC14-amidine bilayers.[58]

In fact, ODN adsorption onto DODAB vesicles simultaneously induces an increase in transition temperature and a decrease in transition cooperativity (Fig. 2). A similar decrease in cooperativity was observed for the superficial adsorption of anionic[59] and cationic[60] polymers to zwitterionic dimyristoylphosphatidylcholine bilayers. In these cases, the cooperativity decrease has been attributed to the formation of polyelectrolyte domains in the membrane.

The thermotropic behavior of DODAB vesicles in the presence of ODN, with an endothermic peak at 54 °C, is similar to the one observed for the coagel phase.[56] Consistent with that, ODN induced coalescence of DODAB vesicles into multilamellar structures (Fig. 3 and 4), as previously described for fluid cationic mixed lipid bilayers.[47,61]

A repeat distance of ~4.5 nm was calculated for the DODAB gel phase in the presence of ODN from SAXS curves (Fig. 4). This distance is much smaller than the ~7.5 nm described for the gel phase of multilamellar DODAB dispersions in water.[55] It is, however, more similar to the ~3.7 nm described for the DODAB coagel phase,[55,62] with the small difference (~0.8 nm) in the repeat distance being consistent with the presence of ODN intercalated between lamellae. Hence, it is reasonable to assume that the ODN induces the formation of a structure that is less hydrated than the gel phase of multilamellar DODAB dispersions in water, and that this structure resembles the dehydrated coagel phase more closely, although no polycrystalline structure is macroscopically observed. In agreement with that, it is known that ODN adsorption to cationic bilayers causes dehydration of the water–lipid interface in a concentration-dependent manner.[63]

The ability of ODN to induce a closer approach between lamellae, with a possible loss of intermediate water, is reinforced by the fact that the repeat distances before (~4.5 nm) and after (~4.8 nm) phase transition are very similar. This contrast with the previously described increase in repeat distances from gel (~7.5 nm) to fluid (~9.2 nm) multilamellar DODAB vesicles.[55] Hence, ODN might act as a bridge between adjacent lamellae.

In fact, the water layer of ~0.5 nm present between two adjacent bilayers (Table 2) is remarkably similar to the ~0.6 nm ODN cross-section. Thus, it is also possible to infer that there is only one ODN layer between two consecutive lamellae. A similar organization was observed using cryo-TEM imaging for multilamellar assemblies of oligonucleotides and cationic DOTAP bilayers.[61]

It is possible to estimate the extended chain length of DODAB from l_{max} (nm) = 0.15 + 0.1265n_c,[64] where n_c is the number of hydrocarbons per lipid chain. For DODAB, l_{max} ~ 2.4 nm, resulting in a bilayer thickness of ~4.8 nm if the alkyl chains are fully extended and without taking into account the lipid polar headgroups. This bilayer thickness is slightly larger than the ~4.5 nm repeat distance calculated for the DODAB gel phase in the presence of ODN (Fig. 4). It is also larger than the 3.4 nm bilayer thickness calculated for the gel phase of 8 mM DODAB in D_2O.[54] There are three possibilities to explain these discrepancies: 1 – the alkyl chains are not fully extended at the gel phase; 2 – the lipid chains are fully extended, but the DODAB molecules are tilted; or 3 – the lipid chains are interdigitated.

The third possibility, that DODAB membranes are interdigitated, can be outright dismissed from the ESR data. In interdigitated membranes, ESR probes located near the bilayer core, such as 16-PCSL, are motionally more restricted and/or ordered than non-interdigitated bilayers and have A_{max} values similar to those of the probes near the bilayer surface, such as 5-PCSL.[36,65,66] That is clearly not the case for DODAB vesicles in the presence or absence of ODN: the A_{max} values for 16-PCSL are much lower than those of 5-PCSL (Fig. 7). The absence of interdigitation might explain why ODN adsorption increases the phase transition temperature for DODAB (Fig. 2) but decreases for diC14-amidine,[58] as previously noted.

The first possibility, that alkyl chains are not fully extended, is supported by the fact that DODAB alkyl chains can be further stretched in the subgel state.[54] As previously noted (Section 3.3.), there is a flexibility gradient towards the bilayer core which is not affected by ODN adsorption (Fig. 5 and 6), showing that even in the gel phase the hydrocarbon chains are not all extended in the all-trans conformation. That is the case for many other lipids.[37] The second possibility, that DODAB molecules are tilted, was reported for supported DODAB multilayers.[67]

The ESR data also show that ODN stabilizes the DODAB gel phase by making it more rigid, *i.e.*, by increasing A_{max} values (Fig. 7). Consistent with the transition temperature increase to 54 °C (Fig. 2), the coexistence of two populations of rigid and fluid lipids observed at the beginning of the gel-fluid transition (40 °C), which had been previously reported,[17] is shifted to 47 °C (Fig. 5 and 6). An increase in DODAB gel-fluid transition temperature was also described for addition of 150 mM NaCl to 4 mM DODAB dispersions.[68] In that case, however, the temperature increase was modest (about 2 °C) when compared to the 10 °C increase observed for the addition of 0.4 mM ODN to 2 mM DODAB (Fig. 2). Although a comparison between monovalent charges and polyelectrolytes is not straightforward,[69] it is possible to infer that the substantial effect of ODN on the gel phase when compared to salt is not caused only by electrostatic interactions with cationic DODAB headgroups. In fact, the stabilization of the gel phase in presence of monovalent salt was only noticed in the bilayer core, since no effect was observed in 5-PCSL spectra.[68] The contrasting increase in gel phase bilayer packing observed with ODN (Fig. 7) could be attributed to superficial dehydration of the bilayers.

In the fluid phase, ODN simultaneously induces a decrease in superficial ordering and an increase in bilayer core packing (Fig. 8). This contrasts with the fact that fluid DODAB bilayers at high salt concentration display a slight decrease in bilayer packing at both the surface and the core,[68] but agrees with the fact that ODN reduces the exposure of hydrophobic bilayer regions to water in fluid cationic bilayers.[63] Hence, dehydration effects caused by ODN could be playing a more important role in fluid bilayer organization than electrostatic effects caused by salt.

The increase in fluid bilayer core packing could explain the decrease in phase transition enthalpy (ΔH) observed in the presence of ODN: in this case, the transition would proceed from a rigid gel phase to a more rigid fluid phase, and the energy difference between gel and fluid phases would be reduced. Consistently, a lower ΔH value was also observed for the gel/fluid transition of diC14-amidine in the presence of ODN, which exhibits a more rigid fluid phase than that of the pure lipid.[53]

5. Conclusions

The structure of DODAB vesicles interacting with oligonucleotides was investigated by means of DSC, SAXS and ESR spectroscopy. The electrostatic adsorption of ODN caused coalescence of unilamellar DODAB vesicles into multilamellar structures with close contact between lamellae. It also caused a substantial increase in phase transition temperature and a decrease in transition cooperativity.

ODN rigidified and stabilized the gel phase. At the fluid phase, a simultaneous decrease in bilayer order close to the surface and increase in bilayer core rigidity was observed in the presence of ODN. These effects may be due not only to the strong electrostatic interactions between anionic ODN phosphates and cationic DODAB headgroups but also to the superficial dehydration of the bilayers.

The set of results presented here demonstrates that the adsorption of highly charged small single-stranded ODNs can deeply affect the structure of cationic DODAB bilayers. Although no polycrystalline structure was observed macroscopically, it is possible that ODNs induce the formation of a multilamellar poorly hydrated coagel-like phase. These effects should be taken in account when planning antisense or vaccine delivery employing cationic bilayer carriers.

Acknowledgements

This work was supported by FAPESP and CNPq. J.H.K.R. is a FAPESP fellow (2011/13079-9). L.R.S.B. and M.T.L. are both recipients of CNPq research fellowships. We thank the Brazilian National Synchrotron Radiation Laboratory (LNLS) staff for help in collecting the SAXS data.

References

1 H. B. Gamper, H. Parekh, M. C. Rice, M. Bruner, H. Youkey and E. B. Kmiec, *Nucleic Acids Res.*, 2000, **28**, 4332–4339.
2 Y. Fichou and C. Férec, *Trends Biotechnol.*, 2006, **24**, 563–570.
3 M. D. De-Backer, B. Nelissen, M. Logghe, J. Viaene, I. Loonen, S. Vandoninck, R. de Hoogt, S. Dewaele, F. A. Simons, P. Verhasselt, G. Vanhoof, R. Contreras and W. H. M. L. Luyten, *Nat. Biotechnol.*, 2001, **19**, 235–241.
4 N. M. Dean, *Curr. Opin. Biotechnol.*, 2001, **12**, 622–625.
5 C. Marwick, *JAMA, J. Am. Med. Assoc.*, 1998, **280**, 871.
6 V. K. Sharma, R. K. Sharma and S. K. Singh, *Med. Chem. Commun.*, 2014, **5**, 1454–1471.
7 L. Liu, X. Zhou, H. Liu, L. Xiang and Z. Yuan, *Immunology*, 2005, **115**, 223–230.
8 D. E. Fonseca and J. N. Kline, *Adv. Drug Delivery Rev.*, 2009, **61**, 256–262.
9 Y. Kuramoto, M. Nishikawa, K. Hyoudou, F. Yamashita and M. Hashida, *J. Controlled Release*, 2006, **115**, 226–233.
10 F. Shi and D. Hoekstra, *J. Controlled Release*, 2004, **97**, 189–209.
11 R. Juliano, M. R. Alam, V. Dixit and H. Kang, *Nucleic Acids Res.*, 2008, **36**, 4158–4171.
12 T. M. Allen and P. R. Cullis, *Adv. Drug Delivery Rev.*, 2013, **65**, 36–48.
13 C. F. Bennett, M. Y. Chiang, H. Chan, J. E. E. Shoemaker and C. K. Mirabelli, *Mol. Pharmacol.*, 1992, **41**, 1023–1033.
14 C. T. Ilarduya, Y. Sun and N. Düzgünes, *Eur. J. Pharm. Sci.*, 2010, **40**, 159–170.
15 A. M. Carmona-Ribeiro and H. Chaimovich, *Biochim. Biophys. Acta*, 1983, **733**, 172–179.
16 L. R. Tsuruta, W. Quintilio, M. H. B. Costa and A. M. Carmona-Ribeiro, *J. Lipid Res.*, 1997, **38**, 2003–2011.
17 C. R. Benatti, E. Feitosa, R. M. Fernandez and M. T. Lamy-Freund, *Chem. Phys. Lipids*, 2001, **111**, 93–104.
18 A. M. Carmona-Ribeiro, *Curr. Med. Chem.*, 2003, **10**, 2425–2446.
19 D. H. W. Hubert, M. Jung and A. L. German, *Adv. Mater.*, 2000, **12**, 1291–1294.
20 D. B. Vieira, L. F. Pacheco and A. M. Carmona-Ribeiro, *J. Colloid Interface Sci.*, 2006, **293**, 240–247.
21 T. R. Oliveira, C. R. Benatti and M. T. Lamy, *Biochim. Biophys. Acta, Biomembr.*, 2011, **1808**, 2629–2637.
22 M. T. N. Campanhã, E. M. Mamizuka and A. M. Carmona-Ribeiro, *J. Phys. Chem. B*, 2001, **105**, 8230–8236.
23 H. Rosa, D. F. S. Petri and A. M. Carmona-Ribeiro, *J. Phys. Chem.*, 2008, **112**, 16422–16430.
24 K. S. Korsholm, E. M. Agger, C. Foged, D. Christensen, J. Dietrich, C. S. Andersen, C. Geisler and P. Andersen, *Immunology*, 2007, **121**, 216–226.
25 J. P. N. Silva, A. C. N. Oliveira, M. P. P. A. Casal, A. C. Gomes, P. J. G. Coutinho, O. P. Coutinho and M. E. C. D. R. Oliveira, *Biochim. Biophys. Acta, Biomembr.*, 2011, **1808**, 2440–2449.
26 J. H. K. Rozenfeld, S. R. Silva, P. A. Ranéia, E. Faquim-Mauro and A. M. Carmona-Ribeiro, *J. Controlled Release*, 2012, **160**, 367–373.
27 O. Schales and S. S. Schales, *J. Biol. Chem.*, 1941, **140**, 879–884.
28 R. M. Fernandez, K. A. Riske, L. Q. Amaral, R. Itri and M. T. Lamy, *Biochim. Biophys. Acta*, 2008, **1778**, 907–916.
29 M. M. Domingues, M. L. Bianconi, L. R. S. Barbosa, P. S. Santiago, M. Tabak, M. A. R. B. Castanho, R. Itri and N. C. Santos, *Biochim. Biophys. Acta*, 2013, **1828**, 2419–2427.
30 R. Zhang, R. M. Suter and J. F. Nagle, *Phys. Rev. E: Stat. Phys., Plasmas, Fluids, Relat. Interdiscip. Top.*, 1994, **50**, 5047–5060.
31 R. Zhang, S. Tristram-Nagle, W. Sun, R. L. Headrick, T. C. Irving, R. M. Suter and J. F. Nagle, *Biophys. J.*, 1996, **70**, 349–357.
32 T. Fruhwirth, G. Fritz, N. Freiberger and O. Glatter, *J. Appl. Crystallogr.*, 2004, **37**, 703–710.
33 P. Andreozzi, S. S. Funari, C. La Mesa, P. Mariani, M. G. Ortore, R. Sinibaldi and F. Spinozzi, *J. Phys. Chem. B*, 2010, **114**, 8056–8060.
34 H. W. Walker and S. B. Grant, *Colloids Surf., A*, 1998, **135**, 123–133.
35 F. Spinozzi, C. Ferrero, M. G. Ortore, A. De Maria Antolinos and P. Mariani, *J. Appl. Crystallogr.*, 2014, **47**, 1132–1139.
36 J. M. Boggs and G. Rangaraj, *Biochim. Biophys. Acta*, 1985, **816**, 221–233.
37 W. L. Hubbell and H. M. McConnell, *J. Am. Chem. Soc.*, 1971, **93**, 314–326.
38 T. Heimburg, *Thermal Biophysics of Membranes*, Wiley-VCH Verlag, Weinheim, 2007.
39 P. Devaux and H. M. McConnell, *J. Am. Chem. Soc.*, 1972, **94**, 4475–4481.
40 O. Glatter and O. Kratky, *Small angle x-ray scattering*, Academic Press, New York, 1982.
41 G. Pabst, M. Rappolt, H. Amenitsch and P. Laggner, *Phys. Rev. E: Stat. Phys., Plasmas, Fluids, Relat. Interdiscip. Top.*, 2000, **62**, 4000–4009.
42 S. Schreier, C. F. Polnaszek and I. C. P. Smith, *Biochim. Biophys. Acta*, 1978, **515**, 375–436.
43 D. Marsh, in *Spin labeling. Theory and applications*, ed. L. J. Berliner and J. Reuben, Plenum Press, New York, 1989, vol. 8, pp. 255–303.
44 C. R. Benatti, R. P. Barroso, C. Lonez, J. M. Ruysschaert and M. T. Lamy, *Biochim. Biophys. Acta*, 2009, **1788**, 1304–1309.
45 J. H. Freed, in *Spin labeling. Theory and applications*, ed. L. J. Berliner, Academic Press, New York, 1976, vol. 1, pp. 53–132.
46 H. Schindler and J. Seelig, *J. Chem. Phys.*, 1973, **59**, 1841–1850.
47 I. Jääskeläinen, B. Sternberg, J. Mönkkönen and A. Urtti, *Int. J. Pharm.*, 1998, **167**, 191–203.
48 M. J. Blandamer, B. Briggs, P. M. Cullis, J. A. Green, M. Waters and G. Soldi, *J. Chem. Soc., Faraday Trans.*, 1992, **88**, 3431–3434.
49 J. Cocquyt, U. Olsson, G. Olofsson and P. Van der Meeren, *Langmuir*, 2004, **20**, 3906–3912.
50 P. Saveyn, P. Van der Meeren, J. Cocquyt, T. Drakenberg, G. Olofsson and U. Olsson, *Langmuir*, 2007, **23**, 10455–10462.
51 L. Coppola, M. Youssry, I. Nicotera and L. Gentile, *J. Colloid Interface Sci.*, 2009, **338**, 550–557.
52 J. Cocquyt, U. Olsson, G. Olofsson and P. Van der Meeren, *Colloid Polym. Sci.*, 2005, **283**, 1376–1381.

53 J. H. K. Rozenfeld, T. R. Oliveira, M. T. Lamy and A. M. Carmona-Ribeiro, *Biochim. Biophys. Acta, Biomembr.*, 2011, **1808**, 649–655.
54 P. Saveyn, P. Van der Meeren, M. Zackrisson, T. Narayan and U. Olsson, *Soft Matter*, 2009, **5**, 1735–1742.
55 F. G. Wu, N. N. Wang and Z. W. Yu, *Langmuir*, 2009, **25**, 13394–13401.
56 F. G. Wu, Z. W. Yu and G. Ji, *Langmuir*, 2011, **27**, 2349–2356.
57 P. C. A. Barreleiro, G. Olofsson and P. Alexandridis, *J. Phys. Chem. B*, 2000, **104**, 7795–7802.
58 J. H. K. Rozenfeld, E. L. Duarte, T. R. Oliveira, C. Lonez, J. M. Ruysschaert and M. T. Lamy, *Langmuir*, 2013, **29**, 11102–11108.
59 Z. V. Feng, S. Granick and A. A. Gewirth, *Langmuir*, 2004, **20**, 8796–8804.
60 M. Sikor, J. Sabin, A. Keyvanloo, M. F. Schneider, J. L. Thewalt, A. E. Bailey and B. J. Frisken, *Langmuir*, 2010, **26**, 4095–4102.
61 S. Weisman, D. Hirsch-Lerner, Y. Barenholz and Y. Talmon, *Biophys. J.*, 2004, **87**, 609–614.
62 M. Jung, A. L. German and H. R. Fischer, *Colloid Polym. Sci.*, 2001, **279**, 105–113.
63 V. M. Meidan, J. S. Cohen, N. Amariglio, D. Hirsch-Lerner and Y. Barenholz, *Biochim. Biophys. Acta*, 2000, **1464**, 251–261.
64 C. Tanford, *J. Phys. Chem.*, 1972, **76**, 3020–3024.
65 J. M. Boggs, G. Rangaraj and A. Watts, *Biochim. Biophys. Acta*, 1989, **981**, 243–253.
66 J. H. K. Rozenfeld, E. L. Duarte, J. M. Ruysschaert, C. Lonez and M. T. Lamy, *Biochim. Biophys. Acta*, 2015, **1848**, 127–133.
67 R. Ionov and A. Angelova, *Thin Solid Films*, 1996, **284–285**, 809–812.
68 C. R. Benatti, R. M. Epand and M. T. Lamy, *Chem. Phys. Lipids*, 2007, **145**, 27–36.
69 F. R. Alves and W. Loh, *J. Colloid Interface Sci.*, 2012, **368**, 292–300.

